RESPONSE ANALYSIS FOR ACTIVE-PASSIVE SEISMIC ISOLATION SYSTEM USING LINEAR MOTORS FOR MONOCRYSTAL PULLERS

Hironori FURUKAWA[1], Takafumi FUJITA[2],
Takayoshi KAMADA[3], and Hideaki MISOKA[4]

ABSTRACT: This paper describes a process of developing a seismic isolation system for monocrystal pullers. In this study, an active isolation system using linear motors has been developed. First, the performance of the system, which reduces the displacement of the monocrystal, was first simulated by simulation analysis. Next, the validity of the isolation system was performed by the shaking table test. The examined result revealed that the active isolation system using linear motors could effectively reduce the displacement of the monocrystal model and the simulation.

Key Words: *Seismic Isolation, Active Isolation, Monocrystal Puller, Linear Motor, Model Matching Method, Simulation Analysis*

INTRODUCTION

In order to manufacture the silicon monocrystal, approximately 90% or more of the monocrystals are grown by the Czochralski (CZ) method. In the CZ process, the seed crystal is immersed in the melting silicon in the crucible and is then withdrawn slowly. A monocrystal forms at the end of the seed crystal and grows longitudinally as it is withdrawn (shown in Figure 1). The monocrystal is suspended by a wire through an extremely narrow neck in a monocrystal puller. The neck is easily broken when a collision occurs between the monocrystal and wall of the puller, even during weak earthquakes.
Currently, passive isolation devices are used to prevent equipment malfunction due to earthquakes. However, in the case of a monocrystal puller, the monocrystal and the wire form a pendulum with a considerably long time period. Due to this resonance factor, passive isolation systems cannot sufficiently reduce the response of the pendulum to the earthquakes. Therefore, an active isolation system is required.
In this study, an active isolation system using linear motors has been developed. The performance of this system, which reduces the displacement of the monocrystal, was simulated by simulation analysis. Shaking table tests were then carried out for a one-dimensional experimental model comprising the isolation device.
These shaking table tests revealed that the active isolation system could effectively reduce the displacement in the monocrystal model and the simulation. The system can function as an active-passive seismic isolation system that can provide not only active isolation to protect the monocrystal from weak earthquakes but also passive isolation to protect the puller from strong earthquakes.

[1] Yacmo Co., Ltd., Tokyo.
[2] Professor, Institute of Industrial Science, The University of Tokyo.
[3] Associate Professor, Tokyo University of Agriculture and Technology.
[4] Postgraduate Student, Tokyo University of Agriculture and Technology.

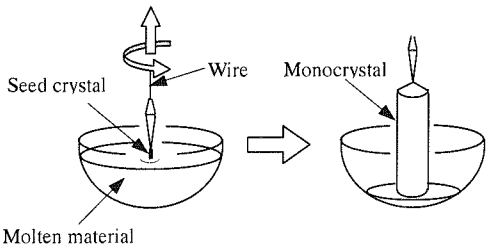

Figure 1. Growth of a monocrystal (CZ method)

MONOCRYSTAL PULLER MODEL AND ACTIVE ISOLATION DEVICE

The experimental model consists of three portions: a seismic isolation device, a monocrystal puller model, and a monocrystal model. The movable frame of the isolation device is supported by four linear bearings and is connected to the base frame by a tension spring and a viscous damper. A linear motor is fixed on the base frame and one end of the column is connected to the movable frame. The maximum displacement of the movable frame is ±245 mm, the natural frequency at the time of all loading is approximately 0.25 Hz, and the attenuation coefficient is approximately 20%. The monocrystal puller model has a cylindrical structure and is 538 kg in mass. The monocrystal model is in the form of a pillar and is 63 kg in mass. It is suspended from the top of the monocrystal puller model by a wire cable, 5 mm in diameter. The natural frequency of the pendulum formed by the wire cable and the monocrystal model is approximately 0.4 Hz (Figure 2).

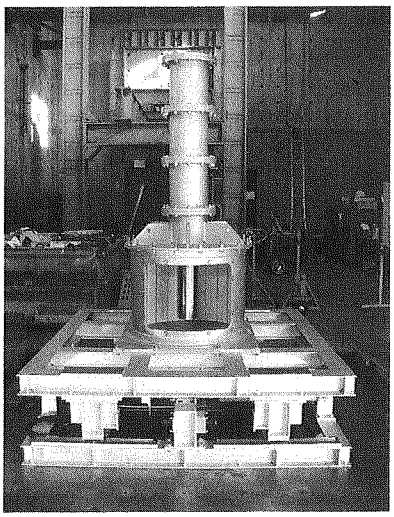

Figure 2. Image of the experimental model

ANALYTICAL MODEL

3-mass/4-degree of freedom system model

The analytical model of the monocrystal puller model and isolation device is shown in Figure 3. In this study, the system was considered to be a 3-mass/4-degree of freedom system of the isolation device, the monocrystal puller model, and the monocrystal model.

The equations of motion are derived as described below:

· kinetic energy of the monocrystal puller:

$$T_1 + T_2 = \frac{1}{2}m_1(\dot{x}_1 + \dot{z})^2 + \frac{1}{2}m_2(\dot{x}_2 + \dot{z})^2 \tag{1}$$

· kinetic energy of the monocrystal:

$$T_3 = \frac{1}{2}m_3(\dot{x}_c{}^2 + \dot{y}_c{}^2) + \frac{1}{2}I_c\dot{\theta}_2{}^2 \tag{2}$$

where x_c, y_c, and I_c represent the displacement in the X and Y direction and the moment of inertia for the center of gravity in the monocrystal.

$$x_c = x_2 + z + l_1\sin\theta_1 + \frac{1}{2}l_2\sin\theta_2 \tag{3}$$

$$y_c = -l_1\cos\theta_1 - \frac{1}{2}l_2\cos\theta_2 \tag{4}$$

$$I_c = m_3\left(\frac{r^2}{4} + \frac{l_2{}^2}{12}\right) \tag{5}$$

Referring to Eqs. (3) and (4)

$$\dot{x}_c{}^2 + \dot{y}_c{}^2 = (\dot{x}_2 + \dot{z})^2 + l_1{}^2\dot{\theta}_1{}^2 + \frac{1}{4}l_2{}^2\dot{\theta}_2{}^2 + 2(\dot{x}_2 + \dot{z})l_1\dot{\theta}_1\cos\theta_1 + (\dot{x}_2 + \dot{z})l_2\dot{\theta}_2\cos\theta_2 + l_1l_2\dot{\theta}_1\dot{\theta}_2\cos(\theta_1 - \theta_2) \tag{6}$$

$$\therefore\ T_3 = \frac{1}{2}m_3(\dot{x}_2 + \dot{z})^2 + \frac{1}{2}m_3l_1{}^2\dot{\theta}_1{}^2 + \frac{1}{2}\left(\frac{1}{4}m_3l_2{}^2 + I_c\right)\dot{\theta}_2{}^2 + m_3(\dot{x}_2 + \dot{z})l_1\dot{\theta}_1\cos\theta_1 + \frac{1}{2}m_3(\dot{x}_2 + \dot{z})l_2\dot{\theta}_2\cos\theta_2 + \frac{1}{2}m_3l_1l_2\dot{\theta}_1\dot{\theta}_2\cos(\theta_1 - \theta_2) \tag{7}$$

Referring to Eqs. (1) and (7), the total kinetic energy T is expressed as follows:

$$\begin{aligned} T &= T_1 + T_2 + T_3 \\ &= \frac{1}{2}m_1(\dot{x}_1 + \dot{z})^2 + \frac{1}{2}(m_2 + m_3)(\dot{x}_2 + \dot{z})^2 + \frac{1}{2}m_3l_1{}^2\dot{\theta}_1{}^2 \\ &\quad + \frac{1}{2}\left(\frac{1}{4}m_3l_2{}^2 + I_c\right)\dot{\theta}_2{}^2 + m_3(\dot{x}_2 + \dot{z})l_1\dot{\theta}_1\cos\theta_1 \\ &\quad + \frac{1}{2}m_3(\dot{x}_2 + \dot{z})l_2\dot{\theta}_2\cos\theta_2 + \frac{1}{2}m_3l_1l_2\dot{\theta}_1\dot{\theta}_2\cos(\theta_1 - \theta_2) \end{aligned} \tag{8}$$

Similarly, the dissipation function is expressed as follows:

$$D = \frac{1}{2}c_1\dot{x}_1{}^2 + \frac{1}{2}c_2(\dot{x}_2 - \dot{x}_1)^2 + \frac{1}{2}c_{\theta1}\dot{\theta}_1{}^2 + \frac{1}{2}c_{\theta2}(\dot{\theta}_2 - \dot{\theta}_1)^2 + \frac{1}{2}c_c(\dot{x}_2 - \dot{x}_1)^2 + \frac{1}{2}c_cl_1{}^2\dot{\theta}_1{}^2 + \frac{1}{8}c_cl_2{}^2\dot{\theta}_2{}^2$$

$$+c_c(\dot{x}_2-\dot{x}_1)l_1\dot{\theta}_1\cos\theta_1+\frac{1}{2}c_c(\dot{x}_2-\dot{x}_1)l_2\dot{\theta}_2\cos\theta_2$$
$$+\frac{1}{2}c_c l_1 l_2\dot{\theta}_1\dot{\theta}_2\cos(\theta_1-\theta_2) \tag{9}$$

Moreover, the potential energy is expressed as follows:

$$U=\frac{1}{2}k_1x_1^2+\frac{1}{2}k_2(x_2-x_1)^2-m_3g(l_1\cos\theta_1+\frac{1}{2}l_2\cos\theta_2) \tag{10}$$

Here, the equations of motion are derived by using Lagrange's equation.

・Lagrange's equations:

$$\frac{d}{dt}\left(\frac{\partial T}{\partial\dot{q}_i}\right)-\frac{\partial T}{\partial q_i}+\frac{\partial U}{\partial q_i}+\frac{\partial D}{\partial q_i}=u_i \tag{11}$$

Since θ_1 and θ_2 are small, the approximation formulas $\sin\theta\approx\theta$, $\cos\theta\approx1$, and $\theta^2\approx0$ are used in the derivation. Further, the attenuation coefficient c_c that acts on the monocrystal model is considered to be the uniformity force of acting f_{cr} using reel type displacement transducer (shown in Figure 4).

Based on the abovementioned process, the equations of motion can be expressed as follows:

$$\ddot{x}_1+\ddot{z}=-\frac{c_1+c_2}{m_1}\dot{x}_1+\frac{c_2}{m_1}\dot{x}_2-\frac{k_1+k_2}{m_1}x_1+\frac{k_2}{m_1}x_2+\frac{1}{m_1}\{u+sign(\dot{x}_c-\dot{x}_1)f_{cr}\} \tag{12}$$

$$\ddot{x}_2+\ddot{z}=\frac{c_2}{m_2}\dot{x}_1-\frac{c_2}{m_2}\dot{x}_2+\frac{k_2}{m_2}x_1-\frac{k_2}{m_2}x_2+\frac{c_{\theta1}+c_{\theta2}}{m_2l_1}\dot{\theta}_1-\frac{c_{\theta2}}{m_2l_1}\dot{\theta}_2+\frac{m_3g}{m_2}\theta_1 \tag{13}$$

$$\begin{aligned}\ddot{\theta}_1=&-\frac{c_2}{m_2l_1}\dot{x}_1+\frac{c_2}{m_2l_1}\dot{x}_2-\frac{k_2}{m_2l_1}x_1+\frac{k_2}{m_2l_1}x_2\\&-\left\{\left(\frac{1}{m_2l_1^2}+\frac{l_2^2}{4l_1^2I_c}+\frac{1}{m_3l_1^2}\right)(c_{\theta1}+c_{\theta2})+\frac{l_2}{2l_1I_c}c_{\theta2}\right\}\dot{\theta}_1\\&+\left(\frac{1}{m_1l_1^2}+\frac{l_2^2}{4l_1^2I_c}+\frac{l_2}{2l_1I_c}+\frac{1}{m_3l_1^2}\right)c_{\theta2}\cdot\dot{\theta}_2-\left(\frac{m_3g}{m_2l_1}+\frac{m_3l_2^2g}{4l_1I_c}+\frac{g}{l_1}\right)\theta_1\\&+\frac{m_3l_2^2g}{4l_1I_c}\theta_2-\frac{1}{m_3l_1}sign(\dot{x}_c-\dot{x}_1)f_{cr}\end{aligned} \tag{14}$$

$$\ddot{\theta}_2=\left(\frac{l_2}{l_1}\cdot\frac{c_{\theta1}+c_{\theta2}}{2I_c}+\frac{c_{\theta2}}{I_c}\right)\dot{\theta}_1-\left(\frac{l_2}{l_1}\cdot\frac{c_{\theta2}}{2I_c}+\frac{c_{\theta2}}{I_c}\right)\dot{\theta}_2+\frac{m_3l_2g}{2I_c}\theta_1-\frac{m_3l_2g}{2I_c}\theta_2 \tag{15}$$

The sliding part of the isolation device experiences friction. Therefore, the state of the device is divided into fixation and operation based on the size of the input seismic wave. In this case, the equations of motion are expressed as given below. The fixation state is Phase 1 and the operation state is Phase 2.

Phase 1: The case wherein the isolation device is fixed by friction

$$\ddot{x}_2 + \ddot{z} = -\frac{c_2}{m_2}\dot{x}_2 + \frac{k_2}{m_2}x_1 - \frac{k_2}{m_2}x_2 + \frac{c_{\theta 1} + c_{\theta 2}}{m_2 l_1}\dot{\theta}_1 - \frac{c_{\theta 2}}{m_2 l_1}\dot{\theta}_2 + \frac{m_3 g}{m_2}\theta_1 \tag{16}$$

$$\begin{aligned}\ddot{\theta}_1 = {} & \frac{c_2}{m_2 l_1}\dot{x}_2 - \frac{k_2}{m_2 l_1}x_1 + \frac{k_2}{m_2 l_1}x_2 - \left\{\left(\frac{1}{m_2 {l_1}^2} + \frac{{l_2}^2}{4{l_1}^2 I_c} + \frac{1}{m_3 {l_1}^2}\right)(c_{\theta 1} + c_{\theta 2}) + \frac{l_2}{2 l_1 I_c}c_{\theta 2}\right\}\dot{\theta}_1 \\ & + \left(\frac{1}{m_1 {l_1}^2} + \frac{{l_2}^2}{4{l_1}^2 I_c} + \frac{l_2}{2 l_1 I_c} + \frac{1}{m_3 {l_1}^2}\right)c_{\theta 2}\cdot\dot{\theta}_2 - \left(\frac{m_3 g}{m_1 l_1} + \frac{m_3 {l_2}^2 g}{4 l_1 I_c} + \frac{g}{l_1}\right)\theta_1 \\ & + \frac{m_3 {l_2}^2 g}{4 l_1 I_c}\theta_2 - \frac{1}{m_3 l_1}sign(\dot{x}_c - x_1)f_{cr}\end{aligned} \tag{17}$$

$$\ddot{\theta}_2 = \left(\frac{l_2}{l_1}\cdot\frac{c_{\theta 1} + c_{\theta 2}}{2I_c} + \frac{c_{\theta 2}}{I_c}\right)\dot{\theta}_1 - \left(\frac{l_2}{l_1}\cdot\frac{c_{\theta 2}}{2I_c} + \frac{c_{\theta 2}}{I_c}\right)\dot{\theta}_2 + \frac{m_3 l_2 g}{2I_c}\theta_1 - \frac{m_3 l_2 g}{2I_c}\theta_2 \tag{18}$$

Phase 2: The case wherein the isolation device is operating

$$\begin{aligned}\ddot{x}_1 + \ddot{z} = {} & -\frac{c_1 + c_2}{m_1}\dot{x}_1 + \frac{c_2}{m_1}\dot{x}_2 - \frac{k_1 + k_2}{m_1}x_1 + \frac{k_2}{m_1}x_2 \\ & + \frac{1}{m_1}(u + sign(\dot{x}_c - \dot{x}_1)f_{cr} - sign(\dot{x}_1)\mu(m_1 + m_2 + m_3)g)\end{aligned} \tag{19}$$

$$\ddot{x}_2 + \ddot{z} = \frac{c_2}{m_2}\dot{x}_1 - \frac{c_2}{m_2}\dot{x}_2 + \frac{k_2}{m_2}x_1 - \frac{k_2}{m_2}x_2 + \frac{c_{\theta 1} + c_{\theta 2}}{m_2 l_1}\dot{\theta}_1 - \frac{c_{\theta 2}}{m_2 l_1}\dot{\theta}_2 + \frac{m_3 g}{m_2}\theta_1 \tag{20}$$

$$\begin{aligned}\ddot{\theta}_1 = {} & -\frac{c_2}{m_2 l_1}\dot{x}_1 + \frac{c_2}{m_2 l_1}\dot{x}_2 - \frac{k_2}{m_2 l_1}x_1 + \frac{k_2}{m_2 l_1}x_2 \\ & - \left\{\left(\frac{1}{m_2 {l_1}^2} + \frac{{l_2}^2}{4{l_1}^2 I_c} + \frac{1}{m_3 {l_1}^2}\right)(c_{\theta 1} + c_{\theta 2}) + \frac{l_2}{2 l_1 I_c}c_{\theta 2}\right\}\dot{\theta}_1 \\ & + \left(\frac{1}{m_1 {l_1}^2} + \frac{{l_2}^2}{4{l_1}^2 I_c} + \frac{l_2}{2 l_1 I_c} + \frac{1}{m_3 {l_1}^2}\right)c_{\theta 2}\cdot\dot{\theta}_2 - \left(\frac{m_3 g}{m_1 l_1} + \frac{m_3 {l_2}^2 g}{4 l_1 I_c} + \frac{g}{l_1}\right)\theta_1 \\ & + \frac{m_3 {l_2}^2 g}{4 l_1 I_c}\theta_2 - \frac{1}{m_3 l_1}sign(\dot{x}_c - x_1)f_{cr}\end{aligned} \tag{21}$$

$$\ddot{\theta}_2 = \left(\frac{l_2}{l_1}\cdot\frac{c_{\theta 1} + c_{\theta 2}}{2I_c} + \frac{c_{\theta 2}}{I_c}\right)\dot{\theta}_1 - \left(\frac{l_2}{l_1}\cdot\frac{c_{\theta 2}}{2I_c} + \frac{c_{\theta 2}}{I_c}\right)\dot{\theta}_2 + \frac{m_3 l_2 g}{2I_c}\theta_1 - \frac{m_3 l_2 g}{2I_c}\theta_2 \tag{22}$$

The conditions for phase change are as follows:

○ Phase 1→Phase 2:

$$\left|m_1\ddot{z} - c_2\dot{x}_2 + (k_1 + k_2)x_1 - k_2 x_2 - u - f_{cr}\right| > \mu(m_1 + m_2 + m_3)g \tag{23}$$

○ Phase 2→Phase 1:

$\dot{x}_1 = 0$ and

$$\left|m_1(\ddot{x}_1+\ddot{z})-c_2\dot{x}_2+(k_1+k_2)x_1-k_2x_2-u-f_{cr}\right|\le\mu(m_1+m_2+m_3)g \tag{24}$$

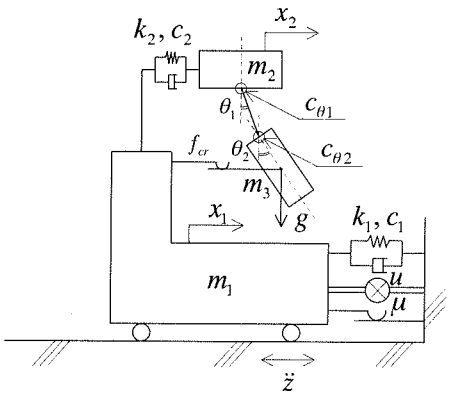

Figure 3. Analytical model

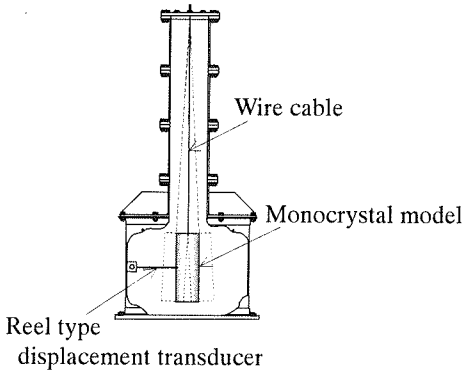

Figure 4. Details of the monocrystal puller model

Identification of the dynamic characteristic of the linear motor

The transfer characteristic from command voltage to an output thrust was measured by inputting the sinusoidal wave, which minced moderately within the limits of a frequency band (0.1–20 [Hz]) as the command signal into the linear motor, and the dynamic characteristic of the linear motor was drawn by curve fitting. The transfer characteristic computed by the experimental result and the dynamic characteristic of the linear motor are shown in Figure 5.

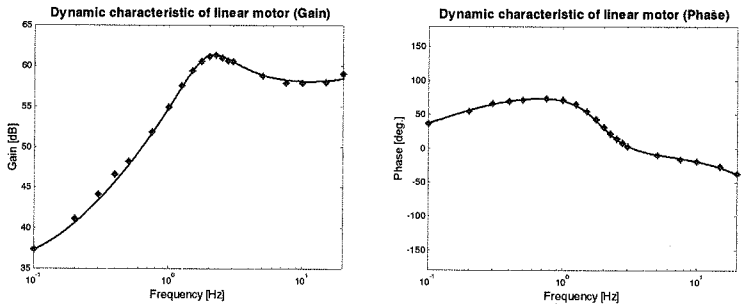

Figure 5. Dynamic characteristic of the linear motor

CONTROL DESIGN

1-mass system model for control design

Since a silicon monocrystal is in a high temperature state of 1000°C or above in a monocrystal puller, it is particularly difficult to directly measure data that is required for control. Hence, the controller for a monocrystal puller was built to operate using only one parameter of the acceleration data in the isolation device. Therefore, the movement model for the control system design is a 1-mass system, as shown in Figure 6. Moreover, since it was difficult to design a controller for a nonlinear model, the friction of the isolation device was neglected and it was treated as an alignment model. However, when considering attenuation by friction, the influence of the fricative is approximated by considering the attenuation coefficient to be larger than the original value.

$$m_1\ddot{x}_1 + \tilde{c}_1\dot{x}_1 + k_1x_1 = F_a - m_1\ddot{z} \tag{25}$$

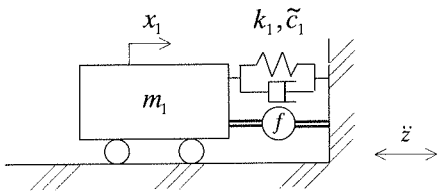

Figure 6. Analytical model for the control system design

Model matching method

In this study, the controller was designed by the model matching method. As a reference, this method designs a closed loop transfer function based on the transfer function of a plant for visual comprehension, and it then computes the control system that realizes it by reverse operation.

Determination of parameters of a controller

The system-wide poles determine a controller. These poles were determined based on the form of W_{dy} and C_{yu}. In this case, W_{dy} and C_{yu} express the closed loop transfer function from the disturbance to the output of the entire system and the frequency characteristic of the conversion into an open loop transfer function from the output of the entire system to a control input, respectively.

W_{dy} is shown in Figure 7.

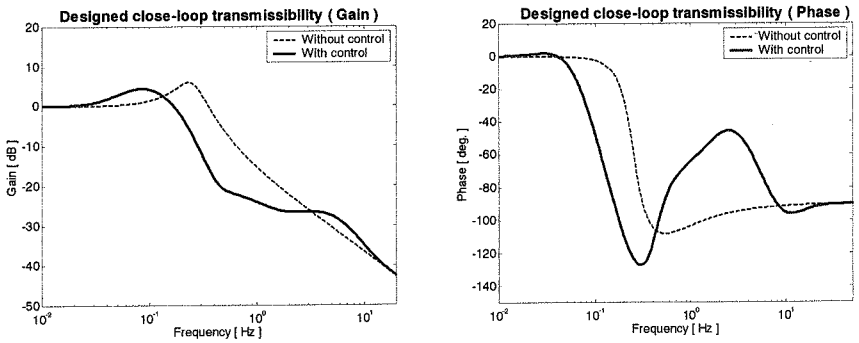

Figure 7. W_{dy}

SIMULATION ANALYSIS

Comparative study by simulation

Using the derived equation, the time history displacements of the monocrystal model when non-isolated and isolated by the passive mode and active mode respectively, were simulated. Two types of earthquake inputs were used in the simulation: ground motion records from El Centro waves (Imperial Valley Earthquake, 1940) and those from JMA Kobe waves (Hyougo-ken Nanbu Earthquake, 1995). The peak accelerations of the earthquake inputs were adjusted to 0.1 and 0.5 m/s^2.

The time history displacements when non-isolated and isolated by the passive modes were simulated; there is very little difference in the amplitude of a monocrystal model because the natural frequency of the isolation device is not sufficiently low as compared with a pendulum. Therefore, passive isolation provides only limited protection to a monocrystal.

On the other hand, active isolation effectively reduces the displacement of the monocrystal model.

The simulation analysis results are shown in Figures 8 and 9.

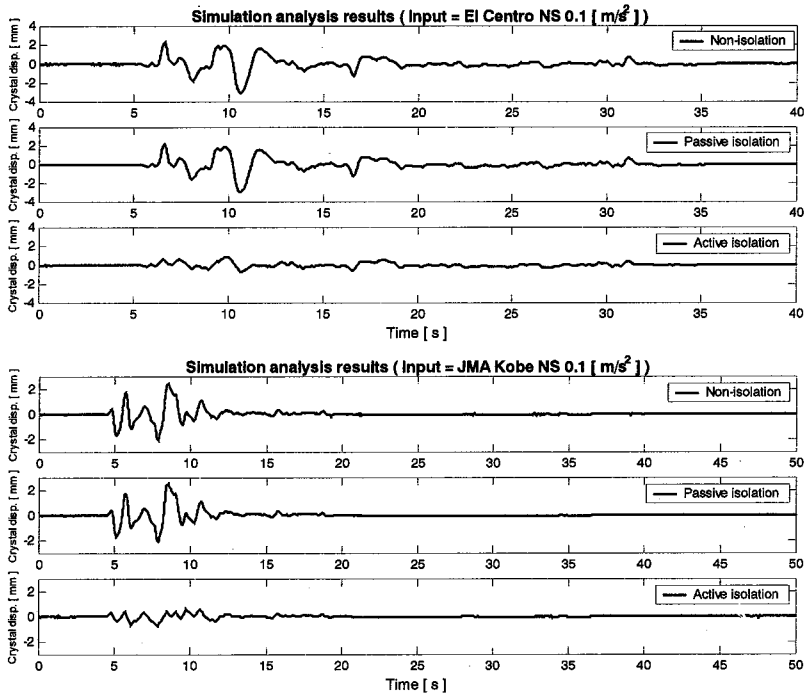

Figure 8. Simulation analysis results (displacement of the monocrystal [Input = 0.1 m/s^2])

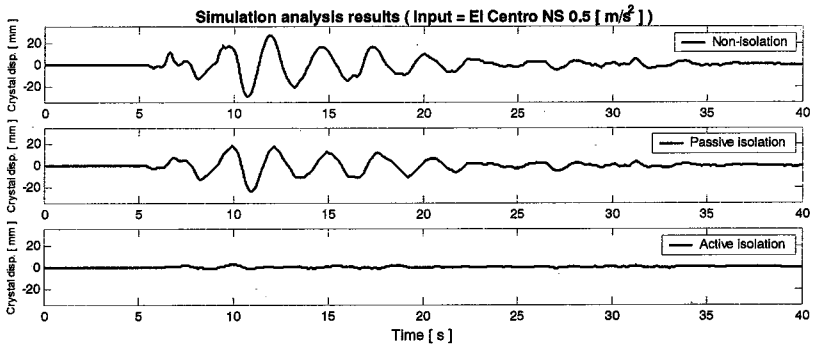

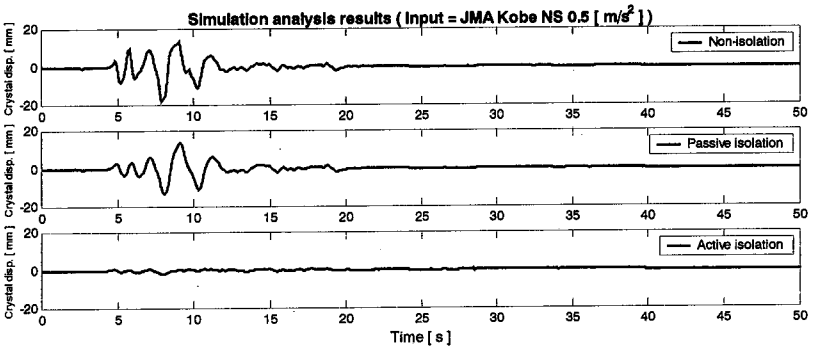

Figure 9. Simulation analysis results (displacement of the monocrystal [Input = 0.5 m/s^2])

EXPERIMENTAL RESULTS

Shaking table tests

In the excitation tests, the two types of earthquake inputs used in the simulation analysis were used. The peak accelerations of the earthquake inputs were adjusted to 0.1 and 0.5 m/s^2.

Figures 10 and 11 show the time history displacements of the monocrystal model when non-isolated and isolated by the passive mode and active mode, respectively.

An observation of the time history displacements when non-isolated, isolated by the passive modes, and by the active modes reveals that same tendency as the simulation result.

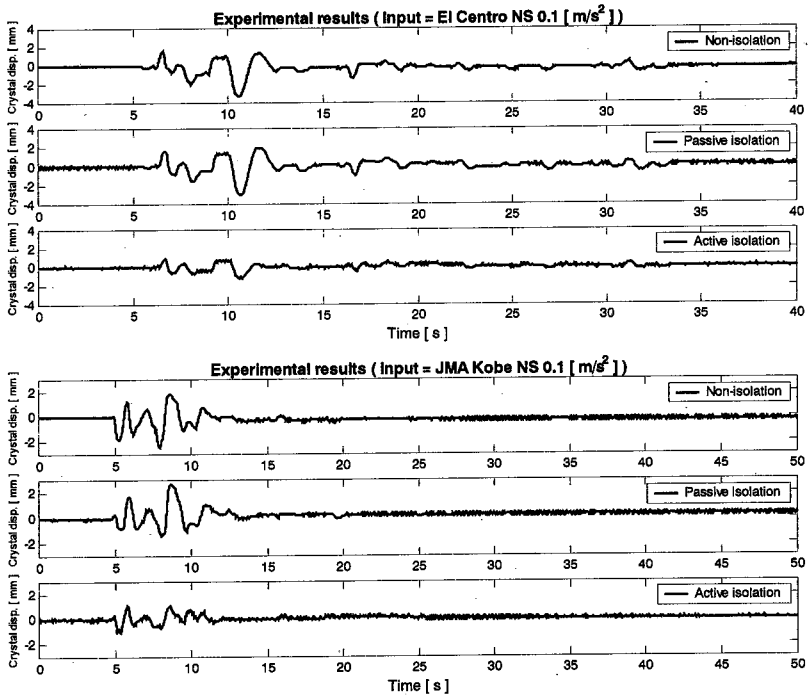

Figure 10. Experimental results (displacement of the monocrystal [Input = 0.1 m/s^2])

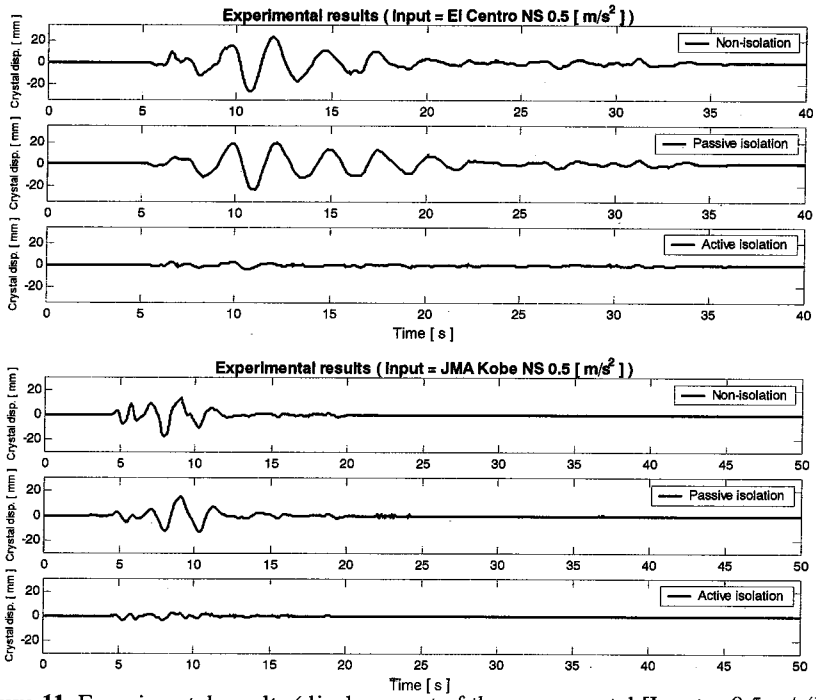

Figure 11. Experimental results (displacement of the monocrystal [Input = 0.5 m/s^2])

Active-Passive modes switching tests

Evidently, when a weak earthquake occurs, the isolation system works as an active isolation device that can effectively protect the monocrystal. Furthermore, the isolation system must automatically switch to the passive mode when a strong earthquake, which exceeds the capacity limit of a linear motor, occurs. The active-passive modes switching tests were carried out in order to verify the variation in isolation performance. When the output of the linear motor exceeded the preset value, the isolation system was set up such that the mode is switched from the active mode to the passive mode. The mode-switching rule was determined such that the mode will switch when the command voltage to the linear motor exceeds 0.75 [V]. Figure 12 shows the time history displacements of the monocrystal model when isolated by the passive mode alone and by the hybrid mode with the active-passive modes switching.

The test results reveal that when the system functions in an active mode, the displacement of the monocrystal model is effectively reduced. On switching to the passive mode, the displacement of the monocrystal model exhibited a response equivalent to the result of the passive isolation experiment. Thus, the effectiveness of the active-passive modes switching was verified based on the protection systems for the motor and the driver.

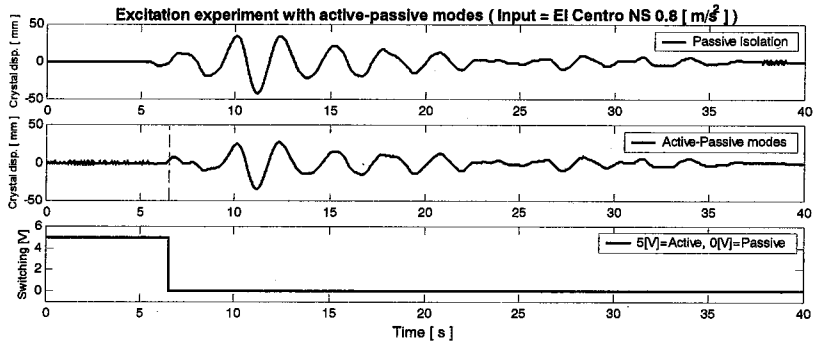

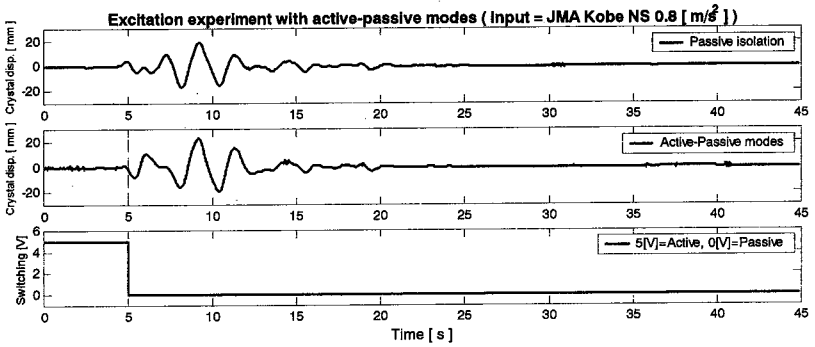

Figure 12. Excitation experiment with active-passive modes (Input = 0.8 m/s^2)

CONCLUSION

A seismic isolation system with convertible active and passive modes has been developed using a linear motor. The performance of the system has been verified by time history displacement of the monocrystal model. The following conclusions have been obtained:

(1) It was possible to simulate the response of the monocrystal to an earthquake almost accurately using the analysis program.

(2) A linear motor used in the active isolation system is effective in preventing the collision of the monocrystal resulting from earthquakes.

(3) It was verified that the active isolation system using a controller designed by the model matching method reduces the displacement of the monocrystal.

(4) The effectiveness of the active-passive modes switching was verified based on the protection systems for the motor and the driver.

REFERENCES

1. T. Fujita, Q. Feng, E. Takenaka, T. Takano, and Y. Suizu, "Active Isolation of Sensitive Equipment for Weak Earthquakes," Proceeding of Ninth World Conference on Earthquake Engineering, Vol.8, SE-10 (1988).
2. T. Fujita, Y. Tagawa, N. Murai, S. Shibuya, A. Takeshita, and Y. Takahashi, "Study of Active Microvibration Control Device Using Piezoelectric Actuator (1st Report, Fundamental Study of One-Dimentional Microvibration Control)," Trans. of the Japan Society of Mechanical Engineers, Vol.57, No.540, Ser. C, (in Japanese) (1991).
3. T. Fujita, K. Tanaka, H. Ohyama, Y. Nakamura, H. Hora, H. Miyano, and M. Suganuma, "Large-Scale Model Experiment of Hybrid Mass Damper with Convertible Active and Passive Modes Using Linear Motor for Vibration Control of Tall Buildings," Trans. of the Japan Society of Mechanical Engineers, Vol.62, No.594, Ser. C, (in Japanese) (1996).
4. T. Fujita, T. Bessho, H. Hora, K. Tanaka and Y. Nakamura, "Control Methods for Active Mass Damper Using Linear Motor for Vibration Control of Tall Buildings," Trans. of the Japan Society of Mechanical Engineers, Vol.64, No.620, Ser. C, (in Japanese) (1998).